IET Generation, Transmission & Distribution

Research Article

IET Journals
The Institution of Engineering and Technology

Enhanced sensitivity-based decentralised framework for real-time transient stability assessment in bulk power grids with renewable energy resources

ISSN 1751-8687
Received on 3rd June 2019
Revised 31st August 2019
Accepted on 12th November 2019
E-First on 9th January 2020
doi: 10.1049/iet-gtd.2019.0848
www.ietdl.org

Mehdi Zareian Jahromi[1], Mohsen Tajdinian[1], Junbo Zhao[2], Payman Dehghanian[3] ✉, Mehdi Allahbakhsi[1], Ali Reza Seifi[1]

[1]*School of Electrical and Computer Engineering, Shiraz University, Shiraz, Iran*
[2]*Department of Electrical and Computer Engineering, Mississippi State University, Starkville, MS, 39759, USA*
[3]*Department of Electrical and Computer Engineering, George Washington University, Washington DC, USA*
✉ *E-mail: payman@gwu.edu*

Abstract: With the increasing trend in the integration and deployment of distributed energy resources, the real-time assessment of power system transient stability is becoming more and more challenging. This study presents an enhanced sensitivity-based decentralised transient stability assessment scheme, which first virtually decomposes the large-scale power network into several smaller areas. Then, a new sensitivity-based scheme is developed to derive and quantify the kinetic energy-based stability assessment index. This index allows taking into account the effects of both AC generators and power electronic-based generator units. In addition, thanks to the new sensitivity-based scheme, the transient stability can be assessed in a decentralised manner using only the boundary buses in each segmented area, which relaxes the need for massive data availability and transfer across the network and enables its applicability for online applications in large-scale power systems. Simulation results on the 48-machine IEEE 140-bus and 544-machine 2000-bus synthetic power grid test systems demonstrate the efficacy of the proposed method.

1 Introduction

With the expanded integration and deployment of the distributed energy resources (DERs), the real-time assessment of power system transient stability (TS) has become more and more challenging [1–3]. In general, TS investigates the ability to preserve the synchronism of the generator rotor angles when a power system is subject to a severe disturbance. In [4], it was shown that with the increased penetration of DERs, the TS margin decreases due to the lower system inertia [5–9].

In the past few decades, TS assessment has been investigated extensively, where the research in this area can be categorised into four groups: (i) time domain simulations (TDS) [10, 11], (ii) transient energy function (TEF) [12–14], (iii) artificial intelligence and machine learning (AI&ML) [15–17], and (iv) hybrid methods [18–23]. In particular, the following challenges (CHs) need to be carefully investigated: CH1 – considering the preservation of the system structure; CH2 – considering fault-on trajectory without post-fault data; CH3 – dealing with multiple and cascading contingencies; CH4 –assessing the stability of the entire power grid; and CH5 – the computational complexity. Several advantages and disadvantages of the aforementioned methods and state-of-the-art research are summarised in Table 1. It can be found that the TDS is able to effectively handle CH1 and CH2, but at the cost of extensive computational burden due to the time-consuming time-domain simulations. Although some efforts have been made in some literature to speed up the process [11], its computational burden is still high as compared to other approaches, such as the one in [21].

Table 1 Advantages and disadvantages of TS methods [10–23].

Approach	Ref.	CHs				
		CH1	CH2	CH3	CH4	CH5
TDS	[10]	✓	✓	✗	✗	very high
	[11]	✓	✓	✗	✗	very high
TEF	[12]	✓	✗	✗	✗	high
	[13]	✓	✗	✗	✗	high
	[14]	✓	✗	✗	✗	high
AI&ML	[15]	✓	✗	✗	✗	low
	[16]	✓	✗	✗	✗	low
	[17]	✓	✗	✗	✗	low
hybrid	[18]	✓	✓	✗	✗	low
	[19]	✓	✗	✗	✗	low
	[20]	✓	✗	✓	✓	low
	[21]	✓	✓	✓	✗	low
	[22]	✓	✓	✗	✗	low
	[23]	✓	✓	✓	✗	low

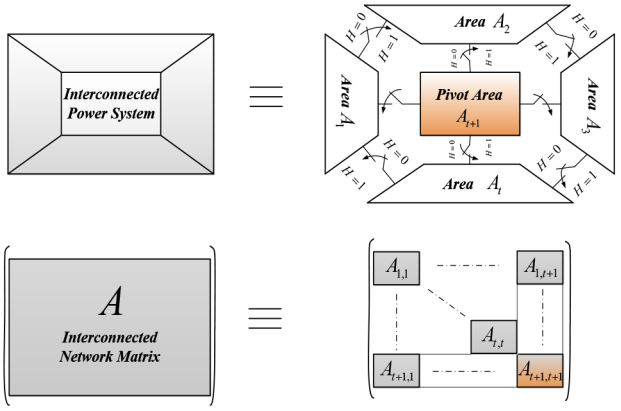

Fig. 1 *Decomposition of large interconnected power network into smaller areas by BBDF method*

TEF and AI&ML techniques can effectively deal with the structure preservation when solving the dynamic equations but at the expense of increased computational burden. Note that the TEF-based methods [12–14] require post-fault data to complete the TS condition assessment. This becomes challenging when considering structure preservation for different types of generation units. Post-fault data are also required for AI&ML-based methods [15–17], where the accuracy relies heavily on the number of contingencies that are utilised to construct and train the model for TS assessment. Both CH3 and CH4 have not been fully addressed in the existing literature. Hybrid methods [18–22] try to integrate the benefits of each method and are mostly based on the kinetic energy; they are designed to deal with TS assessment during fault-on and before fault clearance, yielding more convincing results than those from TEF and AI&ML. Note that the methods proposed in [20, 21, 23] are designed to assess the TS recursively, reflecting the ability to address cascade contingencies without re-simulating the entire set of new contingencies. As a result, they are able to significantly reduce the computational burden in the presence of cascading contingencies. Despite the appealing characteristics of hybrid methods, they require extensive data corresponding to all system generating units for online TS assessment, which is hard to acquire in practice.

While the focus in this study is on real-time assessment of TS in large-scale power systems, it should be mentioned that some algorithms have been developed to speed up the time-domain simulations in power grids, such as the Kron reduction with the diakoptics algorithm presented in [24], the waveform relaxation approaches in [25–27], and parallel-in-time-approaches in [28–30]. In addition, the TDS based on the piece-wise solution of dynamic system equations for large-scale power grids is addressed in [31, 32]. Although the application of parallel computing in power grid TS analysis is focused in the literature, it can be observed that detailed studies on real-time TS assessment considering the large penetration of DERs have still not been fully investigated.

This study develops an enhanced sensitivity-based decentralised TS scheme for large-scale power systems. Our contributions are listed as follows:

- The state-of-the-art techniques for TS assessment in large-scale multi-area power grids require data on all system generating units at each simulation time-step, resulting in massive computational complexity and communication requirements. In response, the proposed method decomposes the network into sub-networks in such a way so that the assessment in multiple regions can be done in parallel. Hence, the decomposition scheme is naturally tailored to fit into a simulation framework and the communications between regions become far less intensive. The proposed decomposition is ideally suited to distribute the computation burden between processors that are used in regional calculations, where each regional processor only needs to access the network data in its own region alone.
- In each sub-network (region), local TS indices are determined and further modified to take into account the boundary interactions between different regions by using a new sensitivity index. This is achieved by integrating the corrected kinetic energy with the large change sensitivity (LCS) method. Note that the corrected kinetic energy index developed in our previous work [20] is extended to consider the effect of fault-on trajectory and other power electronic-based generators in the system.
- In [32], a framework to solve the differential algebraic equations (DAEs) in power grids is developed for time-domain simulations. It solves the TS problem with a reduced computational burden, which is different from the decentralised implementation (DCM) proposed in this study. The commonality between the proposed method and the one presented in [32] is that both methods advocate partitioning the grid to several sub-networks. However, Esmaeili and Kouhsari [32] used LCS for solving piece-wise DAEs during simulation, while the kinetic energy and corrected kinetic energy of each generator are updated in the proposed method based on the sensitivity formulas.

The remaining of this paper is organised as follows: Section 2 describes the proposed approach and steps for its implementation. Simulation results are presented and analysed in Section 3 and Section 4 concludes the paper.

2 Proposed approach

This study aims to present a general and computationally attractive solution to real-time TS monitoring and prediction in large-scale power systems. The key idea is to decompose the system into several small regions and resort to the sensitivity-based approach to derive the TS metrics.

2.1 TS assessment method

There are only a few methods in the literature that are able to effectively address the five CHs introduced earlier (see Table 1), including the one effective approach presented in [21]. However, it suffers from several critical issues as follows: (i) it does not take into account the effects of other power electronic-based generating units; (ii) it is still a centralised approach with significant computational burden and communication requirements since the TS index update needs the information of the entire power grid. The structure-preservation characteristics considered in this method is similar to that in [22], where the sixth-order differential equations for synchronous generators and DFIGs are assumed. The virtual synchronous generator (VSG) [3] is used to model the power electronic-based generator units.

2.2 Decentralised computation

To deal with the computational complexity, this study debates a new challenge in addition to the aforementioned ones, i.e. how to implement a real-time algorithm for TS while reducing the data communication requirement to solve the multi-machine differential equations with ensured accuracy. While the proposed scheme is a parallel processing approach from the calculation viewpoint, it is significantly different from existing state-of-the-art methods to solve the time-domain simulations with different cores and processors [28, 29, 33]. The implementation details of the network decomposition, sensitivity-based analysis, and assessment of the TS index through the proposed decentralised scheme are discussed below.

2.2.1 Block bordered diagonal form (BBDF): The BBDF concept is widely used to characterise a large matrix into a set of several smaller matrices [33] and is used here to decompose a large interconnected power network into several smaller areas. As shown in Fig. 1, the admittance matrix of a large interconnected power network is decomposed into n areas, which are connected to ideal electrical switches (H). Note that the interconnected network is geographically and virtually decomposed so that the areas can be reconnected when ideal switches are closed. Thus, decentralised

processing is possible when the ideal switches are open. After solving the equations separately in each area, the simulation results must be further tuned to account for the effects of other areas. We show in this study that only boundary data are needed to achieve this, where, in particular, the sensitivity analysis-based method is proposed as described below.

2.2.2 Proposed sensitivity analysis approach under decentralised computation: For a large-scale power system, the TS assessment is challenging due to the following reasons:

- The contingencies from neighbouring regions may significantly affect the local power system.
- It is difficult to perform a detailed modelling of the dynamic equations for external power grids since the assessment becomes very time-consuming.

For centralised TS assessments, a set of DAEs of the power system can be generally expressed as follows:

$$\begin{aligned} \dot{z} &= g(z, \boldsymbol{V}) \\ \boldsymbol{I}(z, \boldsymbol{V}) &= \boldsymbol{Y}\boldsymbol{V} \end{aligned} \tag{1}$$

where $\boldsymbol{V}$, $\boldsymbol{I}$, and $\boldsymbol{Y}$ denote the vectors of voltages, the injected current, and the admittance matrix of the power network, respectively. z includes dynamic variables, such as rotor angle, rotor speed etc. For a DCM, it is assumed that in a power system with r number of different regions, the set of DAEs is expressed as follows:

$$\begin{aligned} \dot{z}_1 &= g_1(z_1, V_1),\ I_1(z_1, V_1) = Y_1 V_1 \\ \dot{z}_2 &= g_2(z_2, V_2),\ I_2(z_2, V_2) = Y_2 V_2 \\ &\vdots \\ \dot{z}_r &= g_r(z_r, V_r),\ I_r(z_r, V_r) = Y_r V_r \end{aligned} \tag{2}$$

To solve the aforementioned problem, a decentralised framework is developed with the following three stages:

Stage 1 ($H = 0$): The solutions of dynamic equations in each region at each time step are calculated when the ideal switch is open. As shown in Fig. 1, the areas of a large interconnected power network are connected together via an ideal switch (H) and through their boundary buses. The switch is open when $H = 0$ and it is closed when $H = 1$. Therefore, the Jacobin matrix of the system equations is formulated for the LCS analysis [34] as follows:

$$\frac{\partial \psi(\sigma^k)}{\partial \sigma} = \begin{bmatrix} \frac{\partial \psi_1}{\partial \sigma_1} & & & & \Phi_1 \\ & \frac{\partial \psi_2}{\partial \sigma_2} & & & \Phi_2 \\ & & \ddots & & \vdots \\ & & & \frac{\partial \psi_s}{\partial \sigma_s} & \Phi_s \\ H \cdot \Phi_1^t & H \cdot \Phi_2^t & \cdots & H \cdot \Phi_s^t & (H-1) \cdot \boldsymbol{I} \end{bmatrix} \tag{3}$$

where $[\boldsymbol{\psi}_s]_{n \times m}$ is the Jacobin matrix of the DAEs in each area, σ_s are the independent variables of the system, such as voltage or current in the boundary buses, $[\Phi_s]_{n \times m}$ represents the connections between the smaller areas, and $[\boldsymbol{I}]_{m \times m}$ is the identity matrix. Accordingly, the system Jacobin matrix can be expressed in (4) when all switches are open ($H = 0$) and the state matrix of the system is separately solved for each region as follows:

$$\boldsymbol{\psi}_0 = \frac{\partial \psi(\sigma^k)}{\partial \sigma}\Big|_{H=0} = \begin{bmatrix} \frac{\partial \psi_1}{\partial \sigma_1} & & & & \Phi_1 \\ & \frac{\partial \psi_2}{\partial \sigma_2} & & & \Phi_2 \\ & & \ddots & & \vdots \\ & & & \frac{\partial \psi_s}{\partial \sigma_s} & \Phi_s \\ 0 & 0 & 0 & 0 & -\boldsymbol{I} \end{bmatrix} \tag{4}$$

Stage 2 ($H = 1$): To take into account the effects of interactions between different areas, all ideal switches are closed ($H = 1$) in *Stage 2*. Therefore, the system Jacobin matrix is rewritten as presented in (5)

$$\boldsymbol{\psi} = \frac{\partial \psi(\sigma^k)}{\partial \sigma}\Big|_{H=1} = \begin{bmatrix} \frac{\partial \psi_1}{\partial \sigma_1} & & & & \Phi_1 \\ & \frac{\partial \psi_2}{\partial \sigma_2} & & & \Phi_2 \\ & & \ddots & & \vdots \\ & & & \frac{\partial \psi_s}{\partial \sigma_s} & \Phi_s \\ \Phi_1^t & \Phi_2^t & & \Phi_s^t & \end{bmatrix} \tag{5}$$

In this state, owing to the voltage differences at the boundary buses, the exchange currents ($i_{e\psi}$) between the areas are assessed. As shown in [34], the dynamic solutions in *Stage 1* and the new state matrix of the system should be modified at each time step of simulation as presented in (6)–(8). The new state matrix of the system with state variables (such as rotor angle, exciter voltage, and the other dynamic variables of the system) is then found in (6). Calculation in (6) is straightforward with a low-computational cost because recalculating the inverse of the network matrix is not necessary. Therefore, separate calculations of state variables for each area are achieved via (9)

$$\begin{bmatrix} \xi_1 \\ \xi_2 \\ \vdots \\ \xi_s \\ \xi_{s+1} \end{bmatrix} = \begin{bmatrix} \xi_{10} \\ \xi_{20} \\ \vdots \\ \xi_{s0} \\ 0 \end{bmatrix} - \begin{bmatrix} \left(\frac{\partial \psi_1}{\partial \sigma_1}\right)^{-1} & & & & \left(\frac{\partial \psi_1}{\partial \sigma_1}\right)^{-1} \Phi_1 \\ & \left(\frac{\partial \psi_2}{\partial \sigma_2}\right)^{-1} & & & \left(\frac{\partial \psi_2}{\partial \sigma_2}\right)^{-1} \Phi_2 \\ & & \ddots & & \vdots \\ & & & \left(\frac{\partial \psi_s}{\partial \sigma_s}\right)^{-1} & \left(\frac{\partial \psi_s}{\partial \sigma_s}\right)^{-1} \Phi_s \\ 0 & 0 & 0 & 0 & -\boldsymbol{I} \end{bmatrix} \begin{bmatrix} 0 \\ 0 \\ \vdots \\ 0 \\ I_{e\xi} \end{bmatrix} [\eta_i]_{m \times 1} \tag{6}$$

$$\begin{aligned} [\eta_i]_{m \times 1} &= [\sigma_i]^{-1}_{m \times m} \times [\mu_i]_{m \times n} \times \left[\xi_i^0\right]_{n \times 1} \\ &= \left(\sum_{i=1}^{s} \Phi_i^t \left(\frac{\partial \psi_i}{\partial \sigma_i}\right)^{-1} \Phi_i \right)^{-1}_{m \times m} \times [\mu_i]_{m \times n} \times \left[\xi_i^0\right]_{n \times 1} \end{aligned} \tag{7}$$

$$[\mu_i]_{m \times n} = \left[[\Phi_1]_{m \times t1} \quad [\Phi_2]_{m \times t2} \quad \cdots \quad [\Phi_s]_{m \times ts} \quad \boldsymbol{I}_{m \times m} \right]_{m \times n'} \tag{8}$$

$$[\xi_i] = [\xi_{i0}] - \left[\left(\frac{\partial \xi_i}{\partial \sigma_i} \right) \right]^{-1} [\Phi_i][\mu_i] \tag{9}$$

In the following, the TS index of the system and generators will be modified utilising the proposed sensitivity analysis.

Stage 3: This stage is dedicated to performing a sensitivity analysis on kinetic energy so as to estimate the TS margin of the system and generators via corrected kinetic energy. The kinetic energy of generators and the system is modified while the network state variables are changed by closing ideal switches between the areas. This, in turn, yields

$$\frac{\partial K_{gi}}{\partial \alpha_k} = \frac{1}{2} \times m_i \times \frac{\partial(\varpi_i^2)}{\partial \alpha_k} \tag{10}$$

where K_{gi} is the kinetic energy, ϖ_i is the inertia momentum, α_k is the rotor speed related to each generator, α_k is the dynamic variable of the system, which is changed after closing the ideal switches. The dynamic equation of ϖ_i is based on the network preserving model. Formally, (11) holds

$$M_i \frac{\partial \dot{\omega}_i}{\partial \alpha_k} = -D_i \frac{\partial \omega_i}{\partial \alpha_k} + \frac{\partial P_{mi}}{\partial \alpha_k} - \frac{\partial P_{ei}}{\partial \alpha_k} \tag{11}$$

Note that for the stable equilibrium point of the system, the derivation of dynamic variables, including generator acceleration, is zero [35–37]. Hence, $(\partial \dot{\omega}_i/\partial \alpha_k)$ is zero and $(\partial \omega_i/\partial \alpha_k)$ can be calculated via (12)

$$0 = -D_i \frac{\partial \omega_i}{\partial \alpha_k} + \frac{\partial P_{mi}}{\partial \alpha_k} - \frac{\partial P_{ei}}{\partial \alpha_k} \rightarrow \frac{\partial \omega_i}{\partial \alpha_k} = \frac{1}{D_i}\left(\frac{\partial P_{mi}}{\partial \alpha_k} - \frac{\partial P_{ei}}{\partial \alpha_k}\right) \tag{12}$$

According to (12), it is essential to calculate $(\partial P_{ei}/\partial \alpha_k)$ for synchronous generators, DFIGs, and power electronic-based generators. The mathematical equations of P_e for such units are expressed in (13)–(15), respectively [2, 3, 19]

$$\begin{aligned} P_{ei} = {} & \frac{1}{x'_{di}} E'_{qi} V_i \sin(\delta_i - \theta_i) + \frac{1}{x'_{qi}} E'_{di} V_i \cos(\delta_i - \theta_i) \\ & + \frac{x'_{di} - x'_{qi}}{2 x'_{di} x'_{qi}} V_i^2 \sin[2(\delta_i - \theta_i)] \end{aligned} \tag{13}$$

$$P_{ei} = \frac{1}{x'} E' V_i \sin(\delta_i - \theta_i) \tag{14}$$

$$P_{ei} = \frac{1}{x_{\mathrm{VSG}}} E'_{\mathrm{VSG}} V_i \sin(\delta_i - \theta_i) \tag{15}$$

In (13) and (14), E' and x' are the transient internal voltage and transient reactance, respectively. For synchronous generators, subscript q and d represent the quadrature and direct axis, respectively. For a power electronic-based generator, x_{VSG} is the impedance of the filter reactor. E'_{VSG} is the transient internal voltage. In addition, subscript VSG denotes the virtual synchronous generator. According to (13)–(15), $(\partial P_{ei}/\partial \alpha_k)$ and the sensitivity of the corrected kinetic energy of the generators and the system are modified at each time step of simulation by (16)–(18), respectively

$$\begin{aligned} \frac{\partial P_{ei}}{\partial \alpha_k} = {} & \frac{1}{x'_{di}} \frac{\partial E'_{qi}}{\partial \alpha_k} V_i \sin(\delta_i - \theta_i) + \frac{1}{x'_{di}} E'_{qi} \frac{\partial V_i}{\partial \alpha_k} \sin(\delta_i - \theta_i) \\ & + \frac{1}{x'_{di}} E'_{qi} V_i \left(\frac{\partial \delta_i}{\partial \alpha_k} - \frac{\partial \theta_i}{\partial \alpha_k}\right) \cos(\delta_i - \theta_i) \\ & + \frac{1}{x'_{qi}} \frac{\partial E'_{di}}{\partial \alpha_k} V_i \sin(\delta_i - \theta_i) + \frac{1}{x'_{qi}} E'_{di} \frac{\partial V_i}{\partial \alpha_k} \sin(\delta_i - \theta_i) \\ & - \frac{1}{x'_{qi}} E'_{di} V_i \left(\frac{\partial \delta_i}{\partial \alpha_k} - \frac{\partial \theta_i}{\partial \alpha_k}\right) \sin(\delta_i - \theta_i) \\ & + \frac{x'_{di} - x'_{qi}}{2 x'_{di} x'_{qi}} 2 \frac{\partial V_i}{\partial \alpha_k} V_i \sin[2(\delta_i - \theta_i)] \\ & + 2 \frac{x'_{di} - x'_{qi}}{2 x'_{di} x'_{qi}} V_i^2 \left(\frac{\partial \delta_i}{\partial \alpha_k} - \frac{\partial \theta_i}{\partial \alpha_k}\right) \cos[2(\delta_i - \theta_i)] \end{aligned} \tag{16}$$

$$\begin{aligned} \frac{\partial P_{ei}}{\partial \alpha_k} = {} & \frac{1}{x'} \frac{\partial E'}{\partial \alpha_k} V_i \sin(\delta_i - \theta_i) + \frac{1}{x'} E' \frac{\partial V_i}{\partial \alpha_k} \sin(\delta_i - \theta_i) \\ & + \frac{1}{x'} E' V_i \left(\frac{\partial \delta_i}{\partial \alpha_k} - \frac{\partial \theta_i}{\partial \alpha_k}\right) \cos(\delta_i - \theta_i) \end{aligned} \tag{17}$$

$$\begin{aligned} \frac{\partial P_{ei}}{\partial \alpha_k} = {} & \frac{V_i}{x'_{\mathrm{VSG}}} \frac{\partial E'_{\mathrm{VSG}}}{\partial \alpha_k} \sin(\delta_i - \theta_i) + \frac{E'_{\mathrm{VSG}}}{x'_{\mathrm{VSG}}} \frac{\partial V_i}{\partial \alpha_k} \sin(\delta_i - \theta_i) \\ & + \frac{1}{x'_{\mathrm{VSG}}} E'_{\mathrm{VSG}} V_i \left(\frac{\partial \delta_i}{\partial \alpha_k} - \frac{\partial \theta_i}{\partial \alpha_k}\right) \cos(\delta_i - \theta_i) \end{aligned} \tag{18}$$

2.2.3 Calculating stability index (SI) for each generator and the entire system: In [19], a TS index is proposed which uses the kinetic energy and critical kinetic energy of each generator to calculate the TS margin for each generator. This study suggests utilising corrected critical kinetic energy to define the SI as follows:

$$\mathrm{SI}(t)_{\mathrm{generator},i} = \left\{ \begin{array}{ll} \dfrac{K_g^i(t)}{K_g^{\mathrm{crit},i}(t)}: & t \in \text{Fault duration} \\ \dfrac{K_g^i(t)}{2K_g^{\mathrm{crit},i}(t)}: & t \notin \text{Fault duration} \\ i = 1, 2, \ldots, n; & \end{array} \right\} \tag{19}$$

where $K_g^i(t)$ and $K_g^{\mathrm{crit},i}(t)$ are the kinetic energy and corrected critical kinetic energy for generator i. To calculate SI for the power system, the mathematical expressions of SI for the system and each generator are the same except for the fact that SI for the system utilises $K_{\mathrm{eq}}^{\mathrm{crit}}$ as stated in (20)

$$\mathrm{SI}(t)_{\mathrm{system}} = \left\{ \begin{array}{ll} \dfrac{K_{\mathrm{eq}}(t)}{K_{\mathrm{eq}}^{\mathrm{crit}}(t)}: & t \in \text{Fault duration} \\ \dfrac{K_{\mathrm{eq}}(t)}{2K_{\mathrm{eq}}^{\mathrm{crit}}(t)}: & t \notin \text{Fault duration} \end{array} \right\} \tag{20}$$

In [38], it is mentioned that during a disturbance, the kinetic energy of all generating units does not contribute to the system instability. Therefore, it is essential to calculate effective critical corrected kinetic energy for the entire system. According to [19], the corrected critical kinetic energy is calculated as follows:

$$\left\{ \begin{array}{l} M_{\mathrm{SDG}} = \sum_{i=1}^{n} M_i; \quad i \in \mathrm{SDG} \\ M_{\mathrm{LDG}} = \sum_{i=1}^{n} M_i; \quad i \in \mathrm{LDG} \\ M_{\mathrm{eq}} = \dfrac{M_{\mathrm{SDG}} \times M_{\mathrm{LDG}}}{M_{\mathrm{SDG}} + M_{\mathrm{LDG}}} \end{array} \right\} \tag{21}$$

$$\left\{ \begin{array}{l} \omega_{\mathrm{SDG}}^{\mathrm{crit}} = \dfrac{\sum_{i=1}^{n} M_i \omega_i^{\mathrm{crit}}}{\sum_{i=1}^{n} M_i}; \; i \in \mathrm{SDG} \\ \omega_{\mathrm{LDG}}^{\mathrm{crit}} = \dfrac{\sum_{i=1}^{n} M_i \omega_i^{\mathrm{crit}}}{\sum_{i=1}^{n} M_i}; \; i \in \mathrm{LDG} \\ \omega_{\mathrm{eq}}^{\mathrm{crit}} = \omega_{\mathrm{SDG}}^{\mathrm{crit}} - \omega_{\mathrm{LDG}}^{\mathrm{crit}} \end{array} \right\} \tag{22}$$

$$K_{\mathrm{eq}}^{\mathrm{crit}} = 0.5 \times M_{\mathrm{eq}} \times (\omega_{\mathrm{eq}}^{\mathrm{crit}})^2 \tag{23}$$

As suggested in [38], and in order to take into account the participation of the kinetic energy of the system generators during a fault, the generators are categorised into two groups, namely severely disturbed generator (SDG) and less disturbed generator (LDG). More information regarding SDG and LDG can be found in [38].

Table 2 The generators within each area: IEEE 140-bus test system

area 1	G1, G2, G3, G4, G5, G6, G7, G8, G9, G27, G28, G29, G30
area 2	G10, G11, G12, G13, G14, G15, G16, G17 G18, G19, G20, G21, G22, G23, G26, G31, G33, G34, G35, G36
area 3	G24, G25, G32, G37, G38, G39, G40, G41,G42,G43,G44,G45,G46,G47,G48

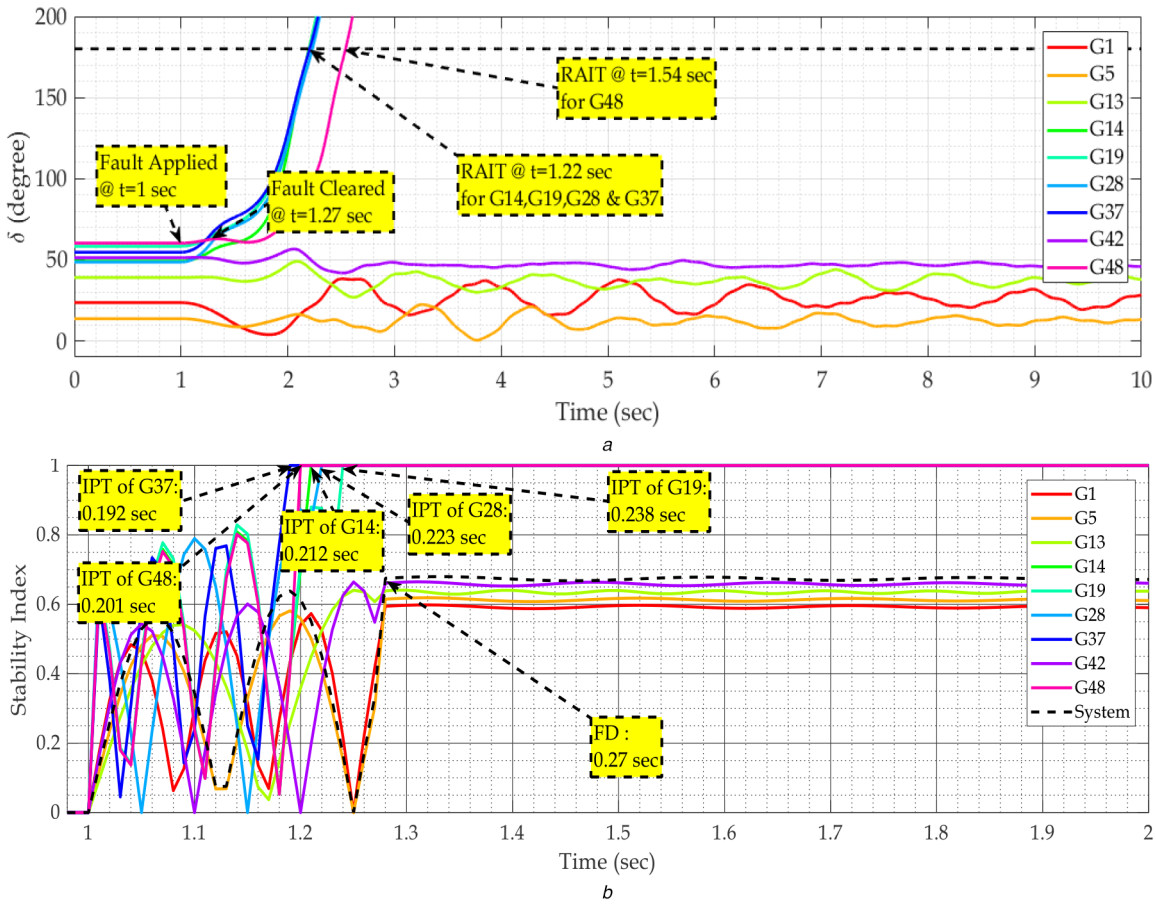

Fig. 2 *Performance evaluation of the proposed method under a three-phase fault applied on bus 29*
(a) Rotor angles of the most critical generators in each area, ***(b)*** Stability indices of generators and the entire power system

3 Simulation results and discussion

In order to evaluate the performance of the proposed method, several case studies are conducted on the 48-machine IEEE 140-bus and 544-machine 2000-bus synthetic power grid test systems. For cases 1 to 3 that are investigated on the IEEE 140-bus test system, it is assumed that the test system is geographically decomposed into three sub-networks. The generators in each area are listed in Table 2 and the test system in each area includes four doubly-fed induction generator (DFIG)-based wind farms with the total 100 MW active power capacity, four photovoltaic (PV) farms with a total 50 MW active power capacity and three superconducting magnetic energy storage (SMES) units with a total 50 MW active power capacity.

3.1 Case 1: performance evaluation under single-order and multi-order contingency scenarios

To investigate the performance of the proposed method under a single contingency scenario, a three-phase fault is applied to bus 29 at $t = 1$ s and cleared at $t = 1.27$ s. The fault duration is randomly selected in this case. As can be seen in Fig. 2*a*, the rotor angles in G14, G19, G28, G37, and G48 appear unstable between 1.2 and 1.5 s after fault instant, while G1, G5, G13, and G28 remain stable. The instability prediction time (IPT) is defined as the duration of time following the fault inception when the SI for a particular generator comes very close to 1. The rotor angle instability time (RAIT) is defined as the duration of time following the fault inception when a generator rotor angle becomes >180° (or < −180°). According to Fig. 2*b*, IPTs for G14, G19, G28, G37, and G48 are 0.212, 0.238, 0.223, 0.192 and 0.201, respectively, while the RAIT for G14, G19, G28, G37 is 1.22 s and for G48 is 1.54 s. Comparing the IPT and RAIT for each generator, it is clear that the proposed method can anticipate the stability condition of the system generators faster than the TDS method. The reason lies in the fact that the proposed method is able to calculate and update the critical corrected kinetic energy in each step of the simulation. The latter enables us to effectively estimate the stability margin of each generator. In addition, the SI of the entire power system anticipates the stability margin of about 63% and it shows that although five system generators experience instability, the kinetic energy of the entire system still holds a 37% margin from the equivalent critical kinetic energy. In other words, the entire system remains stable from the TS point of view. It is worth mentioning that except for the nine generators that are illustrated in Fig. 2, the other 37 generators contribute to the SI.

Since the proposed method recursively assesses the system stability performance, it enables studying the system conditions under multiple-order contingency scenarios. In order to demonstrate this feature, a three-phase fault is applied on bus 109 at $t = 1$ s and cleared at $t = 1.35$ s. Following the fault clearance, the lines between buses 16 and 17, 57 and 70, and 114 and 117 are disconnected at $t = 15$ s. Subsequently, a three-phase fault is applied on bus 109 at $t = 20$ s and cleared at $t = 20.35$ s. Fig. 3*a* displays the rotor angle in this multiple-contingency scenario. It can be found that the rotor angles of the most critical generators remain stable following the first fault scenario. However, after three line outages, generators G4, G30, G31, G32, G33, and G36 become unstable. This observation is confirmed from the SI shown

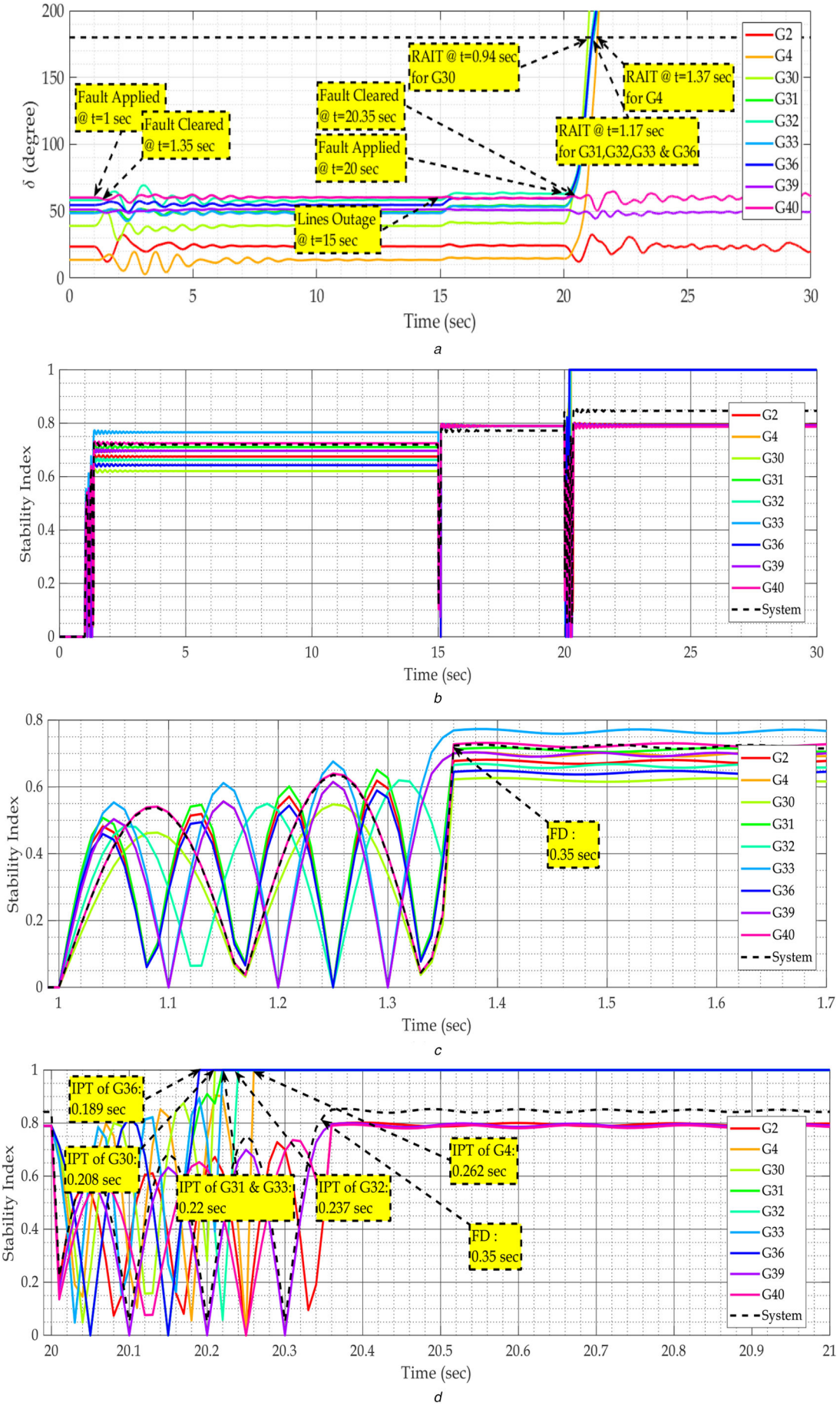

Fig. 3 *Performance evaluation of the proposed method under multi-contingency scenario*

(a) Rotor angles of the most critical generators in each area, ***(b)*** Stability indices of the generators and the entire power system, ***(c)***, ***(d)*** Stability indices of generators and the entire power system before and after the line outage, respectively

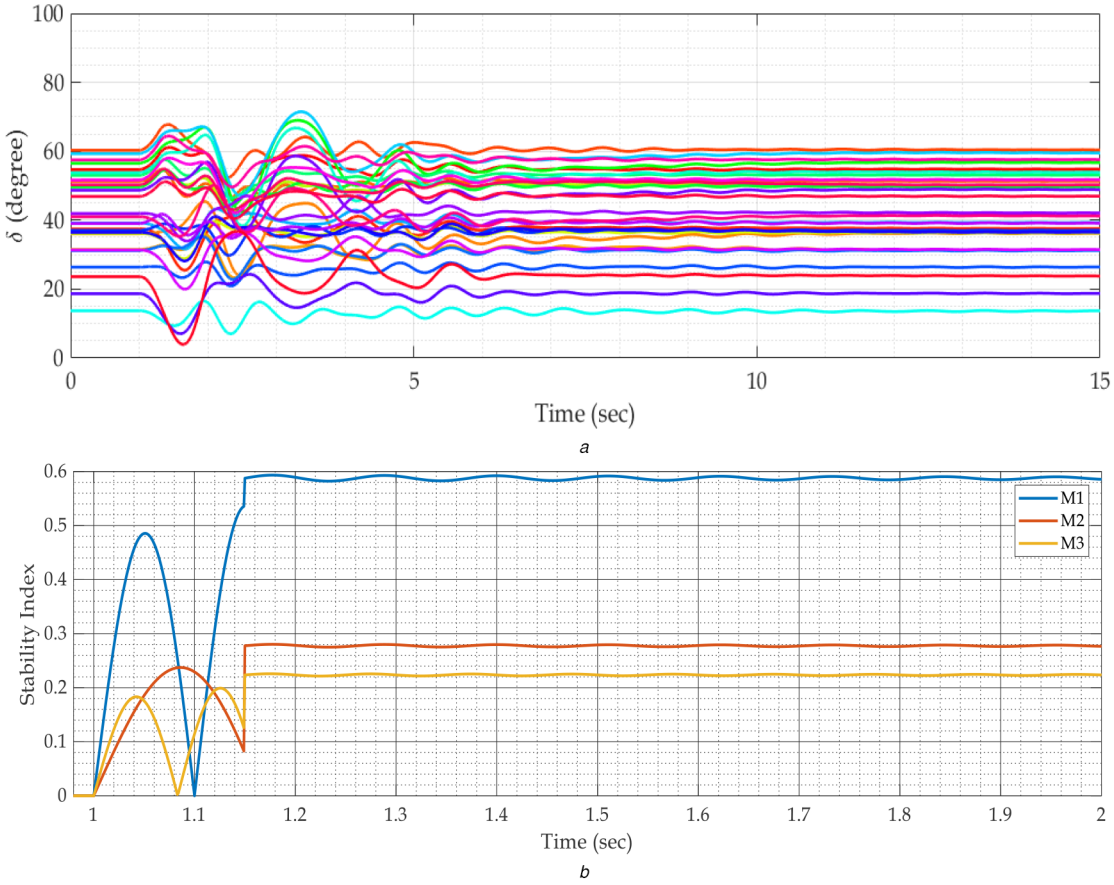

Fig. 4 *Performance evaluation of the proposed method subject to multi-contingency fault scenario handled with different methods*
(a) Rotor angles, ***(b)*** Stability indices of the entire power system

in Fig. 3*b* for each generator. From Fig. 3*c*, one can observe that before the line outages, the SI of each system generator and that of the entire power grid are <1, reflecting the fact that the kinetic energies of the system generators are sufficient in this scenario. Following the line outages, however, the critical kinetic energies of the system generators change and, accordingly, the generators G4, G30, G31, G32, G33, and G36 become unstable. As shown in Fig. 3*d*, the IPTs of generators G4, G30, G31, G32, G33, and G36 vary between 0.19 s and 0.26 s, while the RAITs range between 0.94 and 1.37 s. Comparisons of the IPTs and RAITs under the studied fault scenario and following multiple line outages show that the SI predicts the instability of generators G4, G30, G31, G32, G33, and G36 well earlier than when the rotor angles actually reach 180°. Note that the power grid SI shows almost a stable condition even after the second fault, but as can be seen in Fig. 3*b*, the instability margin is reduced following line outages. Both scenarios demonstrate that the proposed method is able to predict and swiftly track the stability margin of each system generator and the entire power system under contingency scenarios.

3.2 Case 2: investigating the impact of structure-preserving on the SI

This case study is presented to investigate the effects of the structure-preserving criterion on the improvements in the TS index. Increasing penetration of PV generations as well as energy storage systems significantly affects the total system inertia, as well as the level of critical potential and kinetic energy in power grids [3]. To this end, a three-phase fault is applied on bus 126 with a fault duration of 0.15 s. The rotor angles of all generators are given in Fig. 4*a*, where it is clear that all generators remain stable following the fault clearance. The key point in calculating the SI is to find critical corrected kinetic energy that is able to capture the effects of fault-on trajectory, controllers of generators as well as contributions of all effective generators. According to Fig. 4*b*, the SI calculated through the first method (M1) in [20] is near 60%. It should be noted that M1 does not consider the fault-on trajectory in the calculation process of the critical corrected kinetic energy. The second method (M2) proposed in [22] captures the effects of synchronous and induction-based generators. By contrast, the proposed method, namely the third method (M3), takes into account synchronous and induction-based generators and power-electronically connected generators. Since M2 and M3 consider additional details as compared to M1, the stability indices by M2 and M3 are more accurate.

3.3 Case 3: computational efficiency assessment in IEEE140-Bus test system

The computational efficiency of the proposed method is evaluated from two aspects. First, the evaluation is conducted by comparing three different implementations, namely (i) the proposed method with DCM, (ii) centralised version of the proposed method (CM) and (iii) time domain simulation method (TDS). The second evaluation concentrates on the performance of the DCM in TS assessment accuracy and computational complexity. In particular, the performance of the DCM is compared with that of the TDS and [21]. The total simulation time in each case study given in Tables 3 and 4 is assumed to be 10 s.

According to Table 3, it can be concluded that:

- The CPU-time corresponding to the instability estimation using the TDS method varies from 11 to 50 s. The TDS method utilises integration to assess instability time. Based on the fault severity, a fault scenario may result in first swing rotor angle instability. Therefore, the instability time is affected by fault severity and the CPU-time significantly varies accordingly. Except for fault severity, the size of the network has a significant influence on the estimated time of stability as the number of DAEs of a multi-machine system is large to solve.
- In comparison with the TDS method, the CM and DCM schemes have a notable difference in instability time estimation as well as the CPU-time. This significant difference is mainly due to the fact that, in contrast with the TDS method, both CM

and DCM schemes utilise only fault-on data for TS assessment. As a result, CM and DCM are able to estimate the instability time of generators even earlier than the fault clearance, which clearly highlights their ability for real-time applications. On the other hand, the CPU-time corresponding to the CM method is higher than that for the DCM. For instance, according to Table 3 for a fault at bus 22, the instability time 1.195 s is achieved with 1.481 s and 0.5133 s CPU-time for CM and DCM methods, respectively. The DCM resulted in a more promising computational efficiency than the CM even when the same algorithm for TS assessment is utilised.

- In all scenarios, the TDS method has a total CPU-time in the range of 83–85 s. Compared to the TDS method, the CM has a near real-time behaviour with the CPU-time varying around 12 s. The DCM has significantly improved the total CPU-time, yielding 4.7 s thanks to the proposed DCM scheme.

On the other hand, we can draw the following conclusions from Table 4:

- Under different fault locations, it is observed that except for the faults at buses 43 and 92, the method in [21] anticipates a wrong first unstable generator, while the DCM achieves consistent results with the TDS method. This is because the DCM method ensures the network structure-preserving criterion for synchronous machines and PVs with the concept of VSG, which is not the case for the method in [21].
- Both DCM and the method in [21] are able to anticipate generator instability earlier than fault clearance, except for the fact that in most cases, Tajdinian *et al*. [21] identified the wrong unstable generator. Comparing the estimated time of instability with DCM and TDS methods, it is observed that the DCM provides very fast anticipation of the unstable generators. This is because the DCM only utilises during-fault data in its analytical assessment process, while the TDS method identifies unstable generators when the corresponding rotor angle reaches ±180°.
- Regarding the CPU-time, it can be concluded that the DCM provides a relatively low-computational burden as compared to the other methods.

In summary, the DCM is able to provide accurate TS results with a low-computational burden for even large and complex power systems, making it an attractive choice for online applications and real-time decision-making.

3.4 Case 4: computational efficiency assessment in the 2000-bus synthetic power grid

Similar to case 3, the computational efficiency of the proposed framework is evaluated on the 544-machine 2000-bus synthetic power grid [39]. The transmission grid contains 500, 230, 161, and 115 kV voltage levels. More details on the generator types and topology of each area are given in [39]. It is assumed that the studied test system is geographically decomposed into eight areas.

Table 3 Performance evaluation of three different implementations in the IEEE 140-bus test system

Method	Faulted bus#	Time of fault initiation	Time of fault clearance	First unstable generator	Estimated time of instability	CPU-time for estimating instability	CPU-time of simulation
TDS	22	1	1.34	G18	6.10	50.76	83.21
CM					1.195	1.48	12.34
DCM (PM*)					1.195	0.513	4.311
TDS	34	1	1.42	G24	1.420	11.89	83.86
CM					1.284	1.601	12.44
DCM (PM*)					1.284	0.5712	4.57
TDS	120	1	1.73	G32	1.70	14.342	84.25
CM					1.44	1.799	12.52
DCM (PM*)					1.44	0.674	4.71

Table 4 Comparison with the state-of-the-art methods in the IEEE 140-bus test system.

Method	Faulted bus#	Time of fault initiation	Time of fault clearance	First unstable generator	CCT	Estimated time of instability	CPU-time for estimating instability
TDS	43	1	1.23	G26	0.21	4.38	38.71
[21]				G26	0.226	1.226	1.385
DCM (PM*)				G26	0.221	1.221	0.461
TDS	65	1	1.37	G37	0.345	2.394	22.64
[21]				G29	0.294	1.294	2.601
DCM (PM*)				G37	0.361	1.361	0.614
TDS	84	1	1.46	G12	0.415	1.984	47.94
[21]				G23	0.437	1.437	1.37
DCM (PM*)				G12	0.424	1.424	0.533
TDS	92	1	1.52	G35	0.514	5.26	38.97
[21]				G35	0.506	1.506	1.61
DCM (PM*)				G35	0.518	1.518	0.624
TDS	100	1	1.42	G25	0.408	2.367	41.98
[21]				G13	0.368	1.368	1.587
DCM (PM*)				G25	0.411	1.411	0.349
TDS	105	1	1.28	G36	0.264	3.61	52.91
[21]				G7	0.27	1.27	1.31
DCM (PM*)				G36	0.259	1.259	0.43
TDS	117	1	1.39	G41	0.375	2.49	49.51
[21]				G27	0.361	1.361	1.65
DCM (PM*)				G41	0.369	1.369	0.397

Table 5 Performance evaluation of three different implementations in the 2000-bus test system

Method	Faulted bus#	Time of fault initiation	Time of fault clearance	First unstable generator	Estimated instability time	CPU-time for instability	CPU-time of simulation
[32]	1016	1	2.01	G1035	9.81	67.51	145.46
CM					2.43	16.76	139.81
DCM (PM*)					2.43	1.81	7.47
[32]	5395	1	2.24	G3028	9.73	58.84	147.89
CM					2.38	15.96	140.57
DCM (PM*)					2.38	1.78	7.92
[32]	4020	1	2.71	G4052	4.53	35.93	162.51
CM					2.39	9.58	139.72
DCM (PM*)					2.39	1.02	7.26
[32]	5047	1	2.52	G5040	5.48	29.85	159.73
CM					1.84	12.69	139.22
DCM (PM*)					1.84	1.36	7.28
[32]	6035	1	2.36	G6087	7.51	44.02	161.36
CM					2.26	15.58	144.64
DCM (PM*)					2.26	1.67	7.74
[32]	8057	1	2.48	G8147	8.23	48.78	172.87
CM					2.36	16.27	143.10
DCM (PM*)					2.36	1.74	7.67

In each area, about 10% of generators are replaced with DFIG, PV, and SMES with the same generation capacity. Similar to the previous case study, the computational efficiency of the proposed method is compared with the CM and TDS methods. It should be mentioned that the TDS method in this investigation is implemented in a decentralised manner as suggested in [32]. The numerical results are tabulated in Table 5.

The total simulation time in each case study is assumed to be 10 s.

We can observe from Table 5 that the DCM method has the smallest CPU-time for instability assessment and total time simulation as compared to [32] and CM methods. It is worth mentioning that the decentralised calculation in [32] has resulted in reduction of the CPU-time compared to the TDS method presented in Table 3. Similar to Table 3, the estimated times of system instability for both CM and DCM methods are similar, which validates the effectiveness of the DCM. It can also be found that the proposed method reveals less calculation time than that of simulations (total CPU-time is up to 8 s). However, for other methods, the CPU-time is larger than that of simulations. As a result, from the CPU-time point of view, the proposed method can be applied in real-time applications. On the other hand, all simulations are performed on a personal computer. If more computers that are powerful are used, additional saving on the computing time can be achieved.

4 Conclusion

This study proposes a decentralised sensitivity-based scheme for real-time evaluation of TS in large-scale multi-area power grids with different power generation sources. The key idea is to decompose the large-scale network into several small areas and separately assess the TS in each area. This is achieved by developing a new sensitivity-based scheme and the corrected critical kinetic energy index. In addition, the effects of both AC generators and power electronic-based generator units on TS indices are considered. According to the presented case studies, one can conclude that the proposed method is able to monitor, predict, and track the stability condition of each generator and the entire power grid in the presence of various power generation sources. Comparison results with the state-of-the-art methods show that the TS index calculated using the proposed method is further accurate and computationally attractive than its competitors.

5 References

[1] Ahmed, T., Hasanien, H., Alolah, A., *et al.*: 'Transient stability enhancement of a grid-connected wind farm using an adaptive neuro-fuzzy controlled-flywheel energy storage system', *IET Renew. Power Gener.*, 2015, **9**, (7), pp. 792–800

[2] Chowdhury, M.A., Shen, W., Hosseinzadeh, N., *et al.*: 'Quantitative assessment and comparison of fault responses for synchronous generator and wind turbine generators based on modified transient energy function', *IET Renew. Power Gener.*, 2014, **8**, (5), pp. 474–483

[3] Gao, B., Xia, C., Chen, N., *et al.*: 'Virtual synchronous generator based auxiliary damping control design for the power system with renewable generation', *Energies*, 2017, **10**, (8), p. 1146

[4] Oh, S., Shin, H., Cho, H., *et al.*: 'Transient impact analysis of high renewable energy sources penetration according to the future Korean power grid scenario', *Sustainability*, 2018, **10**, (11), p. 4140

[5] Dudurych, I., Burke, M., Fisher, L., *et al.*: 'Operational security challenges and tools for a synchronous power system with high penetration of non-conventional sources', *CIGRE Sci. Eng.*, 2017, **7**, pp. 1-11

[6] Edrah, M., Lo, K.L., Anaya-Lara, O.: 'Impacts of high penetration of DFIG wind turbines on rotor angle stability of power systems', *IEEE Trans. Sustain. Energy*, 2015, **6**, (3), pp. 759–766

[7] Yagami, M., Kimura, N., Tsuchimoto, M., *et al.*: 'Power system transient stability analysis in the case of high-penetration photovoltaics'. 2013 IEEE Grenoble Conf., Grenoble, France, 2013, pp. 1–6

[8] Gautam, D., Vittal, V., Harbour, T.: 'Impact of increased penetration of DFIG-based wind turbine generators on transient and small signal stability of power systems', *IEEE Trans. Power Syst.*, 2009, **24**, (3), pp. 1426–1434

[9] Eftekharnejad, S., Vittal, V., Heydt, G.T., *et al.*: 'Impact of increased penetration of photovoltaic generation on power systems', *IEEE Trans. Power Syst.*, 2012, **28**, (2), pp. 893–901

[10] Kundur, P., Balu, N.J., Lauby, M.G.: '*Power system stability and control*' (McGraw-Hill, New York, NY, USA, 1994)

[11] Wang, C., Yuan, K., Peng, L.I., *et al.*: 'A projective integration method for transient stability assessment of power systems with a high penetration of distributed generation', *IEEE Trans. Smart Grid*, 2018, **9**, (1), pp. 386–395

[12] Vu, T., Turitsyn, K.: 'Lyapunov functions family approach to transient stability assessment', *IEEE Trans. Power Syst.*, 2016, **31**, (2), pp. 1269–1277

[13] Shamisa, A., Karrari, M.: 'Model free graphical index for transient stability limit based on on-line single machine equivalent system identification', *IET Gener. Transm. Distrib.*, 2017, **11**, (2), pp. 314–321

[14] Zhao, S., Jia, H., Fang, D., *et al.*: 'Criterion to evaluate power system online transient stability based on adjoint system energy function', *IET Gener. Transm. Distrib.*, 2014, **9**, (1), pp. 104–112

[15] Gu, X., Li, Y., Jia, J.: 'Feature selection for transient stability assessment based on kernelized fuzzy rough sets and memetic algorithm', *Int. J. Electr. Power Energy Syst.*, 2015, **64**, pp. 664–670

[16] Sulistiawati, I.B., Priyadi, A., Qudsi, O.A., *et al.*: 'Critical clearing time prediction within various loads for transient stability assessment by means of the extreme learning machine method', *Int. J. Electr. Power Energy Syst.*, 2016, **77**, pp. 345–352

[17] Zhang, R., Xu, Y., Dong, Z., *et al.*: 'Post-disturbance transient stability assessment of power systems by a self-adaptive intelligent system', *IET Gener. Transm. Distrib.*, 2015, **9**, (3), pp. 296–305

[18] Jahromi, M., Montaser Kouhsari, S.: 'A high-precision real-time approach to calculate closest unstable equilibrium points', *Int. J. Electr. Power Energy Syst.*, 2017, **89**, pp. 82–93

[19] Jahromi, M., Montaser Kouhsari, S.: 'High speed method for CCT estimation: fundamental, implementation and application in real-time simulation', *Int. J. Emerg. Electr. Power Syst.*, 2017, **18**, (4), pp. 296
[20] Jahromi, M., Montaser Kouhsari, S.: 'A novel recursive approach for real-time transient stability assessment based on corrected kinetic energy', *Appl. Soft Comput.*, 2016, **48**, pp. 660–671
[21] Tajdinian, M., Seifi, A., Allahbakhshi, M.: 'Sensitivity-based approach for real-time evaluation of transient stability of wind turbines interconnected to power grids', *IET Renew. Power Gener.*, 2018, **12**, (6), pp. 668–679
[22] Tajdinian, M., Seifi, A.R., Allahbakhshi, M.: 'Transient stability of power grids comprising wind turbines: new formulation, implementation, and application in real-time assessment', *IEEE Syst. J.*, 2019, **13**, (1), pp. 894–905
[23] Tajdinian, M., Seifi, A., Allahbakhshi, M.: 'Calculating probability density function of critical clearing time: novel formulation, implementation and application in probabilistic transient stability assessment', *Int. J. Electr. Power Energy Syst.*, **103**, (2018), pp. 622–633
[24] Diakoptics, K.G.: '*The piecewise solution of large scale systems*' (McDonald, London, UK, 1963)
[25] Crow, M., Ilic, M.: 'The parallel implementation of the waveform relaxation method for transient stability simulations', *IEEE Trans. Power Syst.*, 1990, **5**, (3), pp. 922–932
[26] Jalili-Marandi, V., Dinavahi, V.: 'Instantaneous relaxation-based real-time transient stability simulation', *IEEE Trans. Power Syst.*, 2009, **24**, (3), pp. 1327–1336
[27] Liu, Y., Jiang, Q.: 'Two-stage parallel waveform relaxation method for large-scale power system transient stability simulation', *IEEE Trans. Power Syst.*, 2016, **31**, (1), pp. 153–162
[28] Alvarado, F.L.: 'Parallel solution of transient problems by trapezoidal integration', *IEEE Trans. Power Appar. Syst.*, 1979, **PAS-98**(3), pp. 1080–1090
[29] La Scala, M., Sblendorio, G., Sbrizzai, R.: 'Parallel-in-time implementation of transient stability simulations on a transputer network', *IEEE Trans. Power Syst.*, 1994, **9**, (2), pp. 1117–1125
[30] Iavernaro, F., La Scala, M., Mazzia, F.: 'Boundary values methods for time-domain simulation of power system dynamic behavior', *IEEE Trans. Circuits Syst. I, Fundam. Theory Appl.*, 1998, **45**, (1), pp. 50–63
[31] Kalantari, A., Kouhsari, S.: 'A distributed computing approach for power system analysis', *Iran. J. Sci. Technol.*, 2005, **29**, pp. 399-413
[32] Esmaeili, S., Kouhsari, S.: 'A distributed simulation based approach for detailed and decentralized power system transient stability analysis', *Electr. Power Syst. Res.*, 2007, **77**, (5), pp. 673–684
[33] Fong, J., Pottle, C.: 'Parallel processing of power system analysis problems via simple parallel microcomputer structures', *IEEE Trans. Power Appar. Syst.*, 1978, **5**, pp. 1834–1841
[34] Vlach, J., Jiří, V., Singhal, K.: '*Computer methods for circuit analysis and design*' (Springer Science & Business Media, Germany, 1983)
[35] Abdel-Azia, F., Vittal, V.: '*Power system transient stability analysis using the transient energy function method*' (Pearson Education, London, UK, 1991)
[36] Pai, M.A., Sauer, P.W., Demaree, K.D.: 'Direct methods of stability analysis in dynamic security assessment', *IFAC Proc.*, 1984, **17**, (2), pp. 2079–2084
[37] Rozenwasser, E., Yusupov, R.: '*Sensitivity of automatic control systems*' (CRC Press, Boca Raton, FL, USA, 1999)
[38] Fang, D.-Z., Chung, T.S., Zhang, Y.*, et al.*: 'Transient stability limit conditions analysis using a corrected transient energy function approach', *IEEE Trans. Power Syst.*, 2000, **15**, (2), pp. 804–810
[39] Xu, T., Birchfield, A., Shetye, K.S.*, et al.*: 'Creation of synthetic electric grid models for transient stability studies'. The 10th Bulk Power Systems Dynamics and Control Symp. (IREP 2017), Espinho, Portugal, 2017, pp. 1–6